

## SHORT COMMUNICATION



## Potent neutralization of SARS-CoV-2 by human antibody heavy-chain variable domains isolated from a large library with a new stable scaffold

Zehua Sun<sup>a\*</sup>, Chuan Chen<sup>a\*</sup>, Wei Li<sup>a\*</sup>, David R. Martinez<sup>b\*</sup>, Aleksandra Drelich<sup>c\*</sup>, Du-San Baek<sup>a</sup>, Xianglei Liu<sup>a</sup>, John W. Mellors<sup>a,d</sup>, Chien-Te Tseng<sup>c</sup>, Ralph S. Baric<sup>b</sup>, and Dimiter S. Dimitrov<sup>a,d</sup><sup>a</sup>Center for Antibody Therapeutics, Division of Infectious Diseases, Department of Medicine, University of Pittsburgh Medical School, Pittsburgh, PA, USA; <sup>b</sup>Department of Epidemiology, University of North Carolina at Chapel Hill, Chapel Hill, NC, USA; <sup>c</sup>Department of Microbiology & Immunology, Centers for Biodefense and Emerging Diseases, Galveston National Laboratory, Galveston, TX, USA; <sup>d</sup>Abound Bio, Pittsburgh, PA, USA**ABSTRACT**

Effective therapies are urgently needed for COVID-19. Here we describe the identification of a new stable human immunoglobulin G1 heavy-chain variable (VH) domain scaffold that was used for the construction of a large library, ICAT6, of engineered human VHs. This library was panned against the receptor-binding domain (RBD) of the SARS-CoV-2 spike (S) glycoprotein. Two VH domains (VH ab6 and VH m397) were selected and fused to Fc for increased half-life in circulation. The VH-Fc ab6 and m397 specifically neutralized SARS-CoV-2 with high potencies (50% neutralization at 0.35 µg/ml and 1.5 µg/ml, respectively) as measured by two independent replication-competent virus neutralization assays. Ab6 and m397 competed with ACE2 for binding to RBD, suggesting a competitive mechanism of virus neutralization. These VH domains may have potential applications for prophylaxis and therapy of COVID-19 alone or in combination, as well as for diagnosis and as tools for research.

**ARTICLE HISTORY**Received 18 May 2020  
Revised Vxx xxx xxxx  
Accepted 20 May 2020**KEYWORDS**Therapeutic antibodies;  
coronaviruses; SARS-CoV-2

### Introduction



As of early 2020, the severe acute respiratory syndrome coronavirus 2 (SARS-CoV-2)<sup>1</sup> has spread worldwide and became a global pandemic.<sup>2,3</sup> Recent statistics showed that more than 3 million people were confirmed positive of virus infection globally, and the number is growing. Safe and effective preventions and therapies are therefore urgently needed. Before an effective vaccine is available, passive antibody therapy will play an important role in medical care. Human monoclonal antibodies (mAbs), which are typically target-specific and nontoxic to humans, are promising therapeutics<sup>4,5</sup> as COVID-19 interventions based on the experience from human mAbs against other emerging viruses, including SARS-CoV, MERS-CoV, and henipaviruses.<sup>6–8</sup> More than 80 antibody therapeutics have been granted marketing approval and more than 570 antibody-derived candidates are being investigated in clinical trials.<sup>9,10</sup> Here, we describe the potent neutralization of SARS-CoV-2 by human VH domains isolated from a large phage-displayed library with a new stable scaffold.

### Results


Phage display is well established among *in vitro* mAb selection technologies,<sup>11–13</sup> and more than 12 antibodies isolated by phage display of different format libraries have been approved for therapy.<sup>14</sup> Human VH domains are relatively small and

could interact with amino acid residues in the target which are not accessible by larger antibody fragments. Importantly, their small size would allow better penetration in normal and diseased tissue. Previously, we demonstrated the construction of a human antibody variable heavy-chain (VH) domain library based on a VH scaffold from IGHV3-23, and isolated neutralizers against HIV-1 from this library.<sup>15</sup> In recent studies, more VH scaffolds, including IGHV3-7, IGHV4-34, IGVH1-69, IGVH3-15, and IGVH5-51, were chosen for library construction based on their frequency in the memory compartment of the immune repertoires.<sup>16,17</sup>

A major concern for generation of VH-based therapeutics is their stability. To identify a relative stable scaffold for VH libraries but without introducing mutations leading to potential immunogenicity we screened natively occurring stable VH scaffolds using a heat denaturation and refolding strategy.<sup>18</sup> We constructed a small VH phage-displayed library (size  $\sim 1 \times 10^7$ ) from 3 healthy human donors' peripheral blood mononuclear cells (PBMCs) and heated it at 80°C for 20 minutes. Chilled phages were spun down and supernatant was collected for bacterial TG1 infection. After three rounds of heating, refolding, and amplification, we evaluated a panel of stable VH scaffolds (Figure 1(a)). One VH scaffold, mCAT1, which is of IGHV3-30, was selected. This scaffold was monomeric as determined by size exclusion chromatography (SEC) (Figure 1(b)) and dynamic light scattering (DLS) (Figure 1(c)). It was stable at 37°C and showed less than 1% aggregation after

**CONTACT** Dimiter S. Dimitrov  [mit666666@pitt.edu](mailto:mit666666@pitt.edu)  ScD Center for Antibody Therapeutics, Division of Infectious Diseases, Department of Medicine, University of Pittsburgh Medical School, Pittsburgh, PA 15261, USA; Zehua Sun [zes20@pitt.edu](mailto:zes20@pitt.edu) Center for Antibody Therapeutics, Division of Infectious Diseases, Department of Medicine, University of Pittsburgh Medical School, S848 Scaife Hall, 3550 Terrace Street, Pittsburgh, PA 15261, USA

\*These authors contributed equally to this work.

 Supplemental data for this article can be accessed on the [publisher's website](#).

© 2020 University of Pittsburgh. Published with license by Taylor & Francis Group, LLC.

This is an Open Access article distributed under the terms of the Creative Commons Attribution-NonCommercial License (<http://creativecommons.org/licenses/by-nc/4.0/>), which permits unrestricted non-commercial use, distribution, and reproduction in any medium, provided the original work is properly cited.

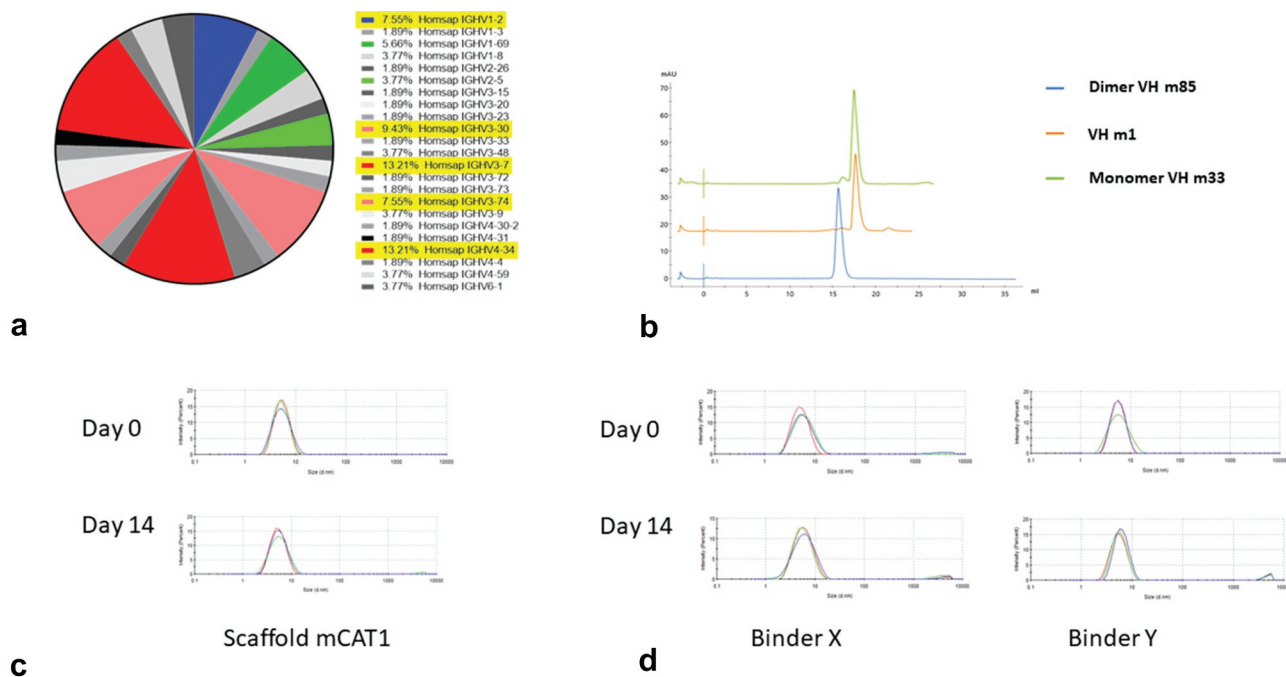


**Figure 1.** Identification and characterization of the mCAT1 scaffold. (a) Isolated human VH genes from multiple heating selection steps. Highly enriched VH frameworks are highlighted in yellow. (b) Size exclusion chromatography profiles for VH (mCAT1, IGHV3-30) scaffold. Known monomeric VH (m33) and dimeric VH (m85) were used for control. (c) Dynamic light scattering analysis for evaluation of the aggregation propensity of the VH (mCAT1) scaffold. The mCAT1 VH was incubated at 37°C for indicated days. Around 4 nm size corresponded to that of a 12.5 kDa VH. (d) Dynamic light scattering analysis of VH binders X and Y. The antibodies were incubated at 37°C for indicated days. Different color curves mean repeats of data reading.

incubation for 14 days (Figure 1(c)). Other highly enriched scaffolds, IGHV3-7, IGHV4-34, are shown in Fig. S1.

A VH domain library, lCAT6, was constructed by grafting naturally occurring CDR2 s and CDR3 s from human PBMCs to mCAT1 as well as to IGHV3-7-, IGHV4-34-, and IGHV3-23-based scaffolds following the strategy described previously.<sup>15</sup> The IGHV3-7-, IGHV4-34-, and IGHV3-23-based scaffolds were added to increase diversity although the mCAT1 scaffold was still dominant representing 40% of the clones. The library construction is shown in Fig.S2. No repeating sequences were found in 100 clones indicating good diversity. In addition, only 21% of the clones were nonproductive (10% of clones had stop codons, and 11% of clones were out of frame). The size of the library was estimated to be  $7.9 \times 10^{10}$  after subtracting the nonproductive clones based on the titration of transformants. The library functionality was tested by panning it against a human protein antigen that is unrelated to the RBD of the SARS-CoV-2 spike protein; two high-affinity binders, VH X and VH Y, were selected which did not aggregate after incubation at 37°C for 14 days as measured by DLS (Figure 1(d)).

We used lCAT6 for the selection of high-affinity VH domains by panning it against recombinant SARS-CoV-2 RBD developed in our laboratory. We identified a panel of binders, two of which, ab6 and m397, were further characterized for affinity, competition with the SARS-CoV-2 receptor ACE2, and neutralization.

Both VH ab6 and m397 bound cell surface-associated native S glycoprotein, confirming that their epitopes are accessible and not changed on the native S protein (Figure 2(a)). The equilibrium dissociation constant,  $K_d$ , of these VH

binders (ab6 and m397) to recombinant RBD as measured by BLItz was 4.6 nM and 29.2 nM, respectively (Figure 2(b)). Both ab6 and m397 competed with ACE2 for binding to the RBD (Figure 3(a)), indicating that the virus could be neutralized by preventing its binding to the receptor. To extend their *in vivo* half-lives and potentially their neutralizing activity, we converted ab6 and m397 to the Fc fusion proteins VH-Fc ab6 and VH-Fc m397, respectively. Both VH-Fc ab6 and VH-Fc m397 bound cell-surface-associated native S glycoprotein (Figure 2(c)). The  $K_d$  of the VH-Fc ab6 and VH-Fc m397 to recombinant RBD as measured by BLItz was 11 nM and 9.6 nM, respectively (Figure 2(d)). Interestingly and rather unusual, the VH-Fc ab6 exhibited higher  $K_d$  (11 nM) to RBD compared to VH ab6 (4.6 nM) mostly due to its significantly decreased association rate constant  $k_a$  – about 10-fold – smaller than that for m397 (about fourfold decrease). Part of this decrease is due to the larger size of the VH-Fc compared to VH resulting from the smaller ratio of the paratope to the total area of the molecule and decreasing the number of effective encounters by Brownian motion as is also for m397. However, significant portion could be due to other factors which remain to be elucidated. In addition, the gain in the dissociation rate constant (about four times, due to avidity because of increased local concentration) for ab6 is smaller than that for m397 which is about 10 times. The unusually large decrease in the association rate constant combined with the relatively small decrease in the dissociation rate constant resulted in the relatively rare situation when avidity of binding is weaker than affinity, one should also take into account that there are two VHs in Fc fusion protein and that avidity depends on the surface concentration of the

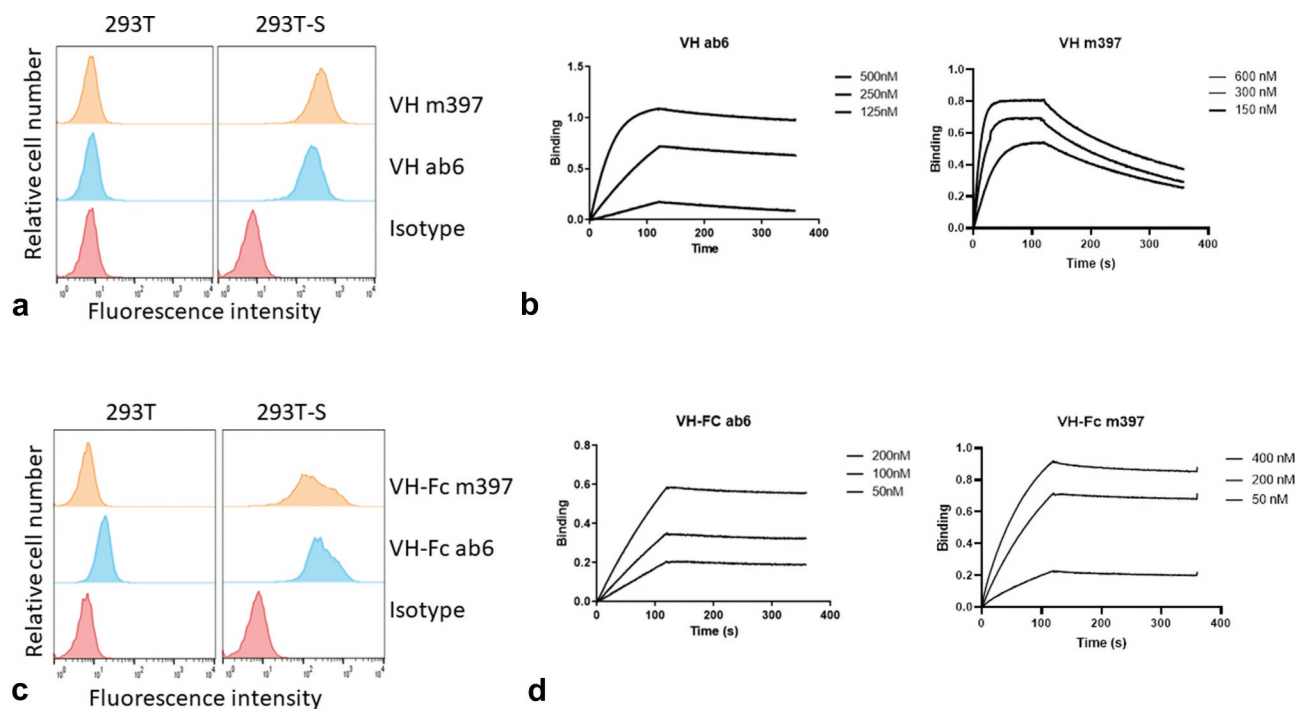


**Figure 2.** Binding characterization of VH ab6 and m397 with or without human IgG1 Fc. (a) Flow cytometry analysis for binding of VH ab6 and m397 to S-glycoprotein expressed on the surface of HEK293 T cell (293 T-S). (b) Representative sensorgrams for VH ab6 and m397. Equilibrium dissociation constants ( $K_d$ ) = 4.6 nM ( $k_a$  = 4.4E4 1/Ms,  $k_d$  = 2.0E-4 1/s) and 29.2 nM ( $k_a$  = 1.3E5 1/Ms,  $k_d$  = 3.9E-3 1/s), respectively. (c) Flow cytometry analysis for binding of VH-Fc ab6 and m397 to S-glycoprotein expressed on the surface of HEK293 T cell. (d) Representative sensorgrams for VH-Fc ab6 and m397. Equilibrium dissociation constants ( $K_d$ ) = 11 nM ( $k_a$  = 4.6E3 1/Ms,  $k_d$  = 5.3E-5 1/s), and 9.6 nM ( $k_a$  = 3.4E4 1/Ms,  $k_d$  = 3.3E-4 1/s), respectively.

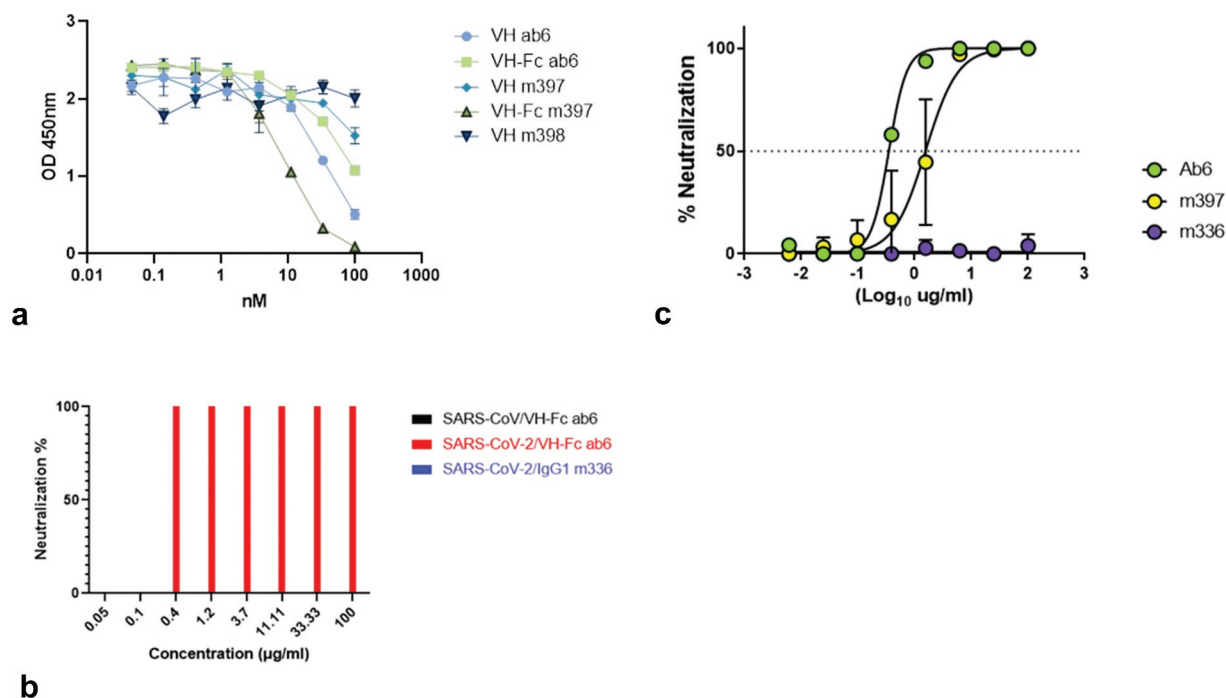


**Figure 3.** Competition with ACE2-Fc and SARS-CoV-2 neutralization activity of ab6 and m397. (a) Competitive ELISA of ACE-Fc binding to plate-immobilized recombinant SARS-CoV-2 RBD in the presence of increasing concentrations of anti-RBD VH ab6 and m397, or VH m398 as a negative control (m398 binds to RBD but does not compete with ACE2). After the competition, bound biotinylated ACE-Fc was detected by SA-HRP. (b) Microneutralization assay. VH-Fc ab6 exhibited significant neutralization activity against SARS-CoV-2 = 100% at 0.4  $\mu\text{g/ml}$  (5.3 nM). Neutralization activity was measured by observation of virus-induced formation of cytopathic effect of Vero E6 cells. The m336 (MERS-CoV neutralizing human IgG1) was used as negative control. (c) Luciferase reporter gene assay for measurement of SARS-CoV-2 neutralizing capacity. The proteins used were Fc-fusions (VH-Fc ab6 and VH-Fc m397). The VH-Fc ab6 and m397 exhibited neutralizing activity against SARS-CoV-2 with high potencies –  $\text{IC}_{50}$  = 0.35  $\mu\text{g/ml}$  (4.6 nM) and 1.5  $\mu\text{g/ml}$  (20 nM), respectively. IgG1 m336 was used as negative control.

target molecules. We plan to study the mechanism of this unusual finding in detail including dose-dependent binding to native S protein expressed in virions and on the cell surface. Consistent with weaker binding compared to VH ab6, VH-Fc ab6 showed decreased competition with ACE2 for binding to RBD compared to VH ab6, while VH-Fc m397 exhibited stronger competition to ACE2 compared to VH m397 due to its enhanced binding avidity to RBD (Figure 3(a)).

VH-Fc ab6 was further characterized by both a standard microneutralization-based assay and a luciferase reporter gene assay to determine its neutralizing activity against live SARS-CoV-2 virus, whereas VH-Fcm397 was evaluated only by the luciferase reporter gene assay. VH-Fc ab6 and VH-Fc m397 exhibited potent activity, neutralizing 50% of the virus at concentrations of 0.35 µg/ml (≈4.6 nM) and 1.5 µg/ml (≈20 nM), respectively, as measured by the luciferase reporter gene assay; VH-Fc ab6 neutralized 100% live virus at 0.4 µg/ml and 0% at 0.1 µg/ml as measured by the microneutralization-based assay (Figure 3(b,c)) which is consistent with the result from the reporter gene assay. In agreement with the specificity of binding to the SARS-CoV-2 RBD and not to the SARS-CoV RBD, neither VH-Fc ab6 nor VH-Fc m397 neutralized live SARS-CoV. One control, our IgG1 m336,<sup>19</sup> which is a potent neutralizer of MERS-CoV (neutralized 50% live MERS-CoV at 0.07 µg/ml), did not exhibit any neutralizing activity against SARS-CoV-2. Interestingly, VH-Fc ab6, which showed weaker competition to ACE2 than VH-Fc m397, more potently neutralized live SARS-CoV-2 than VH-Fc m397, indicating an additional ACE competition independent neutralization mechanism for VH-Fc ab6 which could be through affecting the S protein conformation. This interesting neutralization phenomenon also suggests that ab6 targets a unique epitope on RBD perhaps which could be very different from that of m397. Future experiments are being planned to further characterize the neutralizing activity of these mAbs *in vitro* and *in vivo* alone or in combination with inhibitors as well as to extensively characterize their biophysical properties including their structures in complex with the S protein.

## Discussion

Human antibody VH domains are promising therapeutic candidates. In this study, we constructed a large nonimmune human VH domain antibody phage-displayed library, ICAT6, based on relatively stable VH scaffolds, from which two potent SARS-CoV-2-binding antibodies ab6 and m397 were selected and characterized. Recently, two articles described the isolation of antibody domains against the SARS-CoV-2.<sup>20,21</sup> Those domains were of relatively modest activity and tested only by using pseudovirus assays. The VH-Fc ab6 and m397 exhibited very high inhibitory activity against live virus. VH-Fc ab6 was tested by using two different assays in two different laboratories with essentially the same results. The high affinity/avidity of these mAbs, and their high efficacy in neutralizing live virus, suggest their potential application for prophylaxis and therapy of SARS-CoV-2 infections alone or in combination, as well as for research studies to explore mechanisms of antibody-antigen interactions and for diagnosis.

## Materials and methods

### Library construction and panning

A large phage-displayed human VH library (≈8.9 × 10<sup>10</sup> clones) was constructed by grafting of naturally occurring heavy-chain CDR2 s and CDR3 s from cDNA of a 10 donor-PBMC pool to VH framework scaffolds (Figure 1) as previously described.<sup>15</sup> After library construction, we sequenced 100 clones and did not observe any repetitive sequences, indicating a good diversity of the library. The antibody phage-displayed libraries were preabsorbed on streptavidin-M280-Dynabeads in phosphate-buffered saline (PBS) for 1 h at room temperature (RT) and incubated with 50 nM biotinylated SARS-CoV-2 RBD (residues 330–532) for 2 h at RT with gentle agitation. Phage particles binding to biotinylated antigen were separated from the phage library using streptavidin-M280-Dynabeads and a magnetic separator (Dyna). After washing 20 times with 1 ml of PBS containing 0.1% Tween-20 and another 20 times with 1 ml of PBS, bound phage particles were eluted from the beads using 100 mM triethanolamine followed by neutralization with 1 M, pH7.5 Tris-HCl. For the second round of panning, 10 nM (2 nM for the third round) of biotinylated antigen was used as antigen. After the third round of panning against 2 nM biotinylated antigen, 96 individual clones were screened for binding to RBD-Fc fusion protein by phage ELISA. Panels of VHs were selected and sequenced, and 16 unique sequences were identified.

### Expression, purification of SARS-CoV-2 RBD-his, SARS-CoV-2 RBD-Fc, ACE2-Fc, and VH binders, and conversion of the VH binders to Fc fusion proteins

The gene of SARS-CoV-2 surface glycoprotein was synthesized by IDT (Coralville, Iowa), and the ACE2 gene was ordered from OriGene (Rockville, MD). The sequences were obtained from GenBank® (<https://www.ncbi.nlm.nih.gov/genbank/sars-cov-2-seqs/>). The RBD domain (residues 330–532), S1 domain (residues 14–675), and ACE2 (residues 18–740) genes were cloned into an expression plasmid. This plasmid contains a CMV promoter and woodchuck posttranscriptional regulatory elements, with human IgG1 Fc or His tag, respectively. Proteins were expressed with Expi293 expression system (Thermo Fisher Scientific) and purified with protein A resin (GenScript). Protein purity was estimated as >95% by SDS-PAGE and protein concentration was measured spectrophotometrically (NanoVue, GE Healthcare). For conversion to Fc-fusion, the VH gene was re-amplified and re-cloned into pSectaQ vector (containing human Fc). Protein purity was estimated as >95% by SDS-PAGE and protein concentration was measured spectrophotometrically (NanoVue, GE Healthcare). VH ab6, VH m397, and VH m398 (not published) were in pComb3x vector. Purification of VH binders was performed in *Escherichia coli* HB2151 bacterial culture at 30° C for 16 h with stimulation by 1 mM IPTG. Cells were harvested and lysed by Polymyxin B (Sigma-Aldrich) at 37°C for 0.5 h. Supernatant was loaded over Ni-NTA (GE Healthcare). Purity was estimated to be over 95% by SDS-polyacrylamide gel electrophoresis, and protein concentration was measured spectrophotometrically (NanoVue, GE Healthcare).



## ELISA

Antigen protein was coated on a 96-well plate (Costar) at 50 ng/well in PBS overnight at 4°C. For the soluble VH binding assay, horseradish peroxidase (HRP)-conjugated mouse anti-FLAG tag antibody (A8592, Sigma–Aldrich) was used to detect VH binding. For the competition ELISA, 2 nM of biotinylated human ACE2-Fc was incubated with serially diluted VH or Fc-fused VH, and the mixtures were added to antigen (RBD)-coated wells. After washing, bound biotinylated human ACE2-Fc was detected by HRP-conjugated streptavidin (P9170, Sigma–Aldrich).

## BLItz

Both affinities (ab6 and m397) and avidities (VH-Fc ab6 and VH-Fc m397) of anti-RBD VHs were analyzed by biolayer interferometry BLItz (ForteBio, Menlo Park, CA). To measure affinity, protein A biosensors (ForteBio:18–5010) were coated with RBD-Fc for 2 min and incubated in Dulbecco's PBS (DPBS) (pH = 7.4) to establish baselines. Different doses of VHs were used for association. To measure avidity, RBD-Fc was biotinylated with EZ-link sulfo-NHS-LC-biotin (Thermo Fisher Scientific, Waltham, MA) (RBD-Fc-Bio), and streptavidin biosensors (ForteBio:18–5019) were coated with RBD-Fc-Bio for 2 min and incubated in DPBS (pH = 7.4) to establish baselines. Biosensor only with antibodies and antigen-coated biosensor with PBS were served as reference controls. Different doses of VHs-Fc were recruited for association. The association was monitored for 2 min and dissociation was monitored in DPBS for 4 min.

## Flow cytometry

Full-length S protein of SARS-CoV-2 with replacement of native signal peptide by the CD5 signal peptide was codon-optimized and synthesized (IDT). S gene-containing plasmid was used for transient transfection of 293 T cells cultured in Dulbecco's Modified Eagle's Medium with 10% fetal bovine serum. The transient expression level was tested by fluorescence-activated cell sorting (FACS) using the recombinant hACE2-Fc and IgG1 CR3022. And 1  $\mu$ M antibodies were added to  $1 \times 10^6$  cells for staining. Phycoerythrin (PE)-conjugated anti-human Fc antibody (P9170, Sigma–Aldrich) and viability dye were used to detect antibody-bound cells. For detecting VH antibodies, DYKDDDDK Antibody (130–101-576, Miltenyi Biotec) and viability dye were used. FACS analysis was performed on a BD LSR II (San Jose, CA). Single cells were gated first, followed by gating of live cells. PE-A+ population was gated based on live cells. FACS binding analysis was performed using FlowJo\_V10\_CL.

## Micro-neutralization assay

The standard live virus-based microneutralization assay was used for measurement.<sup>22</sup> Serially diluted test antibodies were prepared in 96-well microtiter plates with a final volume of 60  $\mu$ l per well before adding 120 infectious units of SARS-CoV or SARS-CoV-2 in 60  $\mu$ l to individual wells. After 2 h culturing

at room temperature, 100  $\mu$ l of the antibody-virus mixtures were transferred into designated wells of confluent Vero E6 cells grown in 96-well microtiter plates. Vero E6 cells with or without virus infection served as positive and negative controls, and Vero E6 cells treated with the MERS-CoV RBD-specific neutralizing m336 mAb were included as an additional control. Virus-induced formation of cytopathic effect was detected by microscopy after four days of incubation at 37°C. The work was performed in the Department of Microbiology & Immunology, Centers for Biodefense and Emerging Diseases, Galveston National Laboratory, 301 University Blvd, Galveston, Texas 77550, USA.

## Reporter gene neutralization assay

Full-length viruses expressing luciferase were designed and recovered.<sup>23</sup> Viruses were titered in Vero E6 USAMRID cells before experiments. Vero E6 USAMRID cells were plated at 20,000 cells per well in clear-bottom black-walled 96-well plates (Corning 3904) one day before experiments. Antibody samples were fourfold serially diluted from 100  $\mu$ g/ml. SARS-CoV-UrbaniLuc and SARS-CoV-2-SeattlenLuc viruses were mixed with serially diluted antibodies according to the University of North Carolina safety rules and were incubated at 37°C with 5% CO<sub>2</sub> for one hour. After incubation, growth media was removed from cells and virus-antibody dilution complexes were added to the cells. Virus-only controls and cell-only controls were included in each assay. After infection, cells were incubated at 37°C with 5% CO<sub>2</sub> for 48 hours and then were lysed and luciferase activity was measured via Nano-Glo Luciferase Assay System (Promega). Experiments were performed in duplicate and IC<sub>50</sub> was analyzed by Graphpad Prism 7 under “sigmoidal dose-response (variable slope)” equation.

## Acknowledgments

We would like to thank the members of the Center for Antibody Therapeutics Doncho Zhelev, Cynthia Adams and Xiaojie Chu for their help with some of the experiments and helpful discussions. We also thank Rui Gong from the Institute of Virology in Wuhan and Rachel Fong from Integral Molecular for helpful suggestions. This work was supported by the University of Pittsburgh Medical Center. David R. Martinez is funded by an NIH NIAID T32 AI007151 and a Burroughs Wellcome Fund Postdoctoral Enrichment Program Award. RSB is supported by grants from the NIH AI132178 and AI108197. Some monoclonal antibodies were generated by the University of North Carolina Protein Expression and Purification core facility, which is funded by NIH grant P30CA016086.

## Author contributions

DSD, RSB, CTT, JWM and ZS conceived and designed the research; ZS and WL identified and characterized antibodies; CC made recombinant antigens and characterized them; DB and XL made and characterized reagents and performed some of the experiments; AD and DM performed the neutralization assays; DSD and ZS wrote the first draft of the article, and all authors discussed the results and contributed to the manuscript.

## Disclosure of Potential Conflicts of Interest

No potential conflicts of interest were disclosed.

## Funding

This work was supported by the University of Pittsburgh Medical Center. [University of Pittsburgh Medical Center.]; NIH [AI132178 and AI108197].

## References

- Zhou P, Yang X-L, Wang X-G, Hu B, Zhang L, Zhang W, Si H-R, Zhu Y, Li B, Huang C-L, et al. A pneumonia outbreak associated with a new coronavirus of probable bat origin. *Nature*. 2020;579:270–73. doi:10.1038/s41586-020-2012-7.
- Schuklenk U. COVID19: why justice and transparency in hospital triage policies are paramount. *Bioethics*. 2020;34:325–27. doi:10.1111/bioe.12744.
- Thao TTN, Labroussaa F, Ebert N, V'kovski P, Stalder H, Portmann J, Kelly J, Steiner S, Holwerda M, Kratzel A, et al. Rapid reconstruction of SARS-CoV-2 using a synthetic genomics platform. *Nature*. 2020. doi:10.1038/s41586-020-2294-9.
- Chen L, Xiong J, Bao L, Shi Y. Convalescent plasma as a potential therapy for COVID-19. *Lancet Infect Dis*. 2020;20:398–400. doi:10.1016/S1473-3099(20)30141-9.
- Hoffmann M, Kleine-Weber H, Schroeder S, Krüger N, Herrler T, Erichsen S, Schiergens TS, Herrler G, Wu N-H, Nitsche A, et al. SARS-CoV-2 cell entry depends on ACE2 and TMPRSS2 and is blocked by a clinically proven protease inhibitor. *Cell*. 2020;181:271–280.e8. doi:10.1016/j.cell.2020.02.052.
- Zhu Z, Dimitrov AS, Bossart KN, Crameri G, Bishop KA, Choudhry V, Mungall BA, Feng Y-R, Choudhary A, Zhang M-Y, et al. Potent neutralization of Hendra and Nipah viruses by human monoclonal antibodies. *J Virol*. 2006;80:891–99. doi:10.1128/JVI.80.2.891-899.2006.
- Zhu Z, Bossart KN, Bishop KA, Crameri G, Dimitrov AS, McEachern JA, Feng Y, Middleton D, Wang L-F, Broder CC, et al. Exceptionally potent cross-reactive neutralization of Nipah and Hendra viruses by a human monoclonal antibody. *J Infect Dis*. 2008;197:846–53. doi:10.1086/528801.
- Prabakaran P, Gan J, Feng Y, Zhu Z, Choudhry V, Xiao X, Ji X, Dimitrov DS. Structure of severe acute respiratory syndrome coronavirus receptor-binding domain complexed with neutralizing antibody. *J Biol Chem*. 2006;281:15829–36. doi:10.1074/jbc.M600697200.
- Iyer S, Zaheer S, Vandre D, Long C, Montgomery R. Characterization of human interferon species using gel extraction and monoclonal antibodies: implications on clinical use of interferon preparations. *J Biol Response Mod*. 1986;5:548–61.
- Kung PC, Berger CL, Estabrook A, Edelson RL. Monoclonal antibodies for clinical investigation of human T lymphocytes. *Int J Dermatol*. 1983;22:67–74. doi:10.1111/j.1365-4362.1983.tb03318.x.
- Kumar R, Pararray HA, Shrivastava T, Sinha S, Luthra K. Phage display antibody libraries: a robust approach for generation of recombinant human monoclonal antibodies. *Int J Biol Macromol*. 2019;135:907–18. doi:10.1016/j.ijbiomac.2019.06.006.
- Ubah O, Palliyil S. Monoclonal antibodies and antibody like fragments derived from immunised phage display libraries. *Adv Exp Med Biol*. 2017;1053:99–117. doi:10.1007/978-3-319-72077-7\_6.
- Bhardwaj D, Singh SS, Abrol S, Chaudhary VK. Monoclonal antibodies against a minor and the major coat proteins of filamentous phage M13: their application in phage display. *J Immunol Methods*. 1995;179:165–75. doi:10.1016/0022-1759(94)00280-a.
- Lu RM, Hwang Y-C, Liu I-J, Lee -C-C, Tsai H-Z, Li H-J, Wu H-C. Development of therapeutic antibodies for the treatment of diseases. *J Biomed Sci*. 2020;27:1. doi:10.1186/s12929-019-0592-z.
- Chen W, Zhu Z, Feng Y, Dimitrov DS. Human domain antibodies to conserved sterically restricted regions on gp120 as exceptionally potent cross-reactive HIV-1 neutralizers. *Proc Natl Acad Sci USA*. 2008;105:17121–26. doi:10.1073/pnas.0805297105.
- Van Blarcom T, Lindquist K, Melton Z, Cheung WL, Wagstrom C, McDonough D, Valle Oseguera C, Ding S, Rossi A, Potluri S, et al. Productive common light chain libraries yield diverse panels of high affinity bispecific antibodies. *mAbs*. 2018;10:256–68. doi:10.1080/19420862.2017.1406570.
- Tiller T, Schuster I, Deppe D, Siegers K, Strohn R, Herrmann T, Berenguer M, Poujol D, Stehle J, Stark Y, et al. A fully synthetic human Fab antibody library based on fixed VH/VL framework pairings with favorable biophysical properties. *mAbs*. 2013;5:445–70. doi:10.4161/mabs.24218.
- Dudgeon K, Rouet R, Kokmeijer I, Schofield P, Stolp J, Langley D, Stock D, Christ D. General strategy for the generation of human antibody variable domains with increased aggregation resistance. *Proc Natl Acad Sci USA*. 2012;109:10879–84. doi:10.1073/pnas.1202866109.
- Ying T, Du L, Ju TW, Prabakaran P, Lau CCY, Lu L, Liu Q, Wang L, Feng Y, Wang Y, et al. Exceptionally potent neutralization of Middle East respiratory syndrome coronavirus by human monoclonal antibodies. *J Virol*. 2014;88:7796–805. doi:10.1128/JVI.00912-14.
- Wu Y, Li C, Xia S, Tian X, Kong Y, Wang Z, Gu C, Zhang R, Tu C, Xie Y, et al. Identification of human single-domain antibodies against SARS-CoV-2. *Cell Host Microbe*. 2020. doi:10.1016/j.chom.2020.04.023.
- Wrapp D, De Vlieger D, Corbett KS, Torres GM, Wang N, Van Breedam W, Roose K, van Schie L, Hoffmann M, Pöhlmann S, et al. Structural basis for potent neutralization of betacoronaviruses by single-domain camelid antibodies. *Cell*. 2020;181:1004–1015.e15. doi:10.1016/j.cell.2020.04.031.
- Agrawal AS, Ying T, Tao X, Garron T, Algaissi A, Wang Y, Wang L, Peng B-H, Jiang S, Dimitrov DS, et al. Passive transfer of A germline-like neutralizing human monoclonal antibody protects transgenic mice against lethal Middle East respiratory syndrome coronavirus infection. *Sci Rep*. 2016;6:31629. doi:10.1038/srep31629.
- Scobey T, Yount BL, Sims AC, Donaldson EF, Agnihothram SS, Menachery VD, Graham RL, Swanstrom J, Bove PF, Kim JD, et al. Reverse genetics with a full-length infectious cDNA of the Middle East respiratory syndrome coronavirus. *Proc Natl Acad Sci U S A*. 2013;110:16157–62. doi:10.1073/pnas.1311542110.